Computers and Concrete, *Vol. 12, No. 1 (2013) 65-77*
DOI: http://dx.doi.org/10.12989/cac.2013.12.1.065

Damage analysis of arch dam under blast loading

Xinhua Xue*[1], Xingguo Yang[1] and Wohua Zhang[2]

[1]*College of Water Resource and Hydropower, Sichuan University, Chengdu, P.R. China.*
[2]*MOE Key Laboratory of Soft Soils and Geoenvironmental Engineering, Zhejiang University, Hangzhou, P.R. China.*

(Received August 26, 2012, Revised December 4, 2012, Accepted January 3, 2013)

Abstract. This paper examines the dynamic response of an arch dam subjected to blast loading. A damage model is developed for three dimensional analysis of arch dams. The modified Drucker-Prager criterion is adopted as the failure criteria of the damage evolution in concrete. Then, Xiluodu arch dam serves as an example to simulate the failure behaviors of structures with the proposed model. The results obtained using the proposed model can reveal the reliability degree of the safe operation level of the high arch dam system as well as the degree of potential failure, providing a reliable basis for risk assessment and risk control.

Keywords: damage; blast loading; response; risk control

1. Introduction

Hydropower is a more environmental friendly way of producing electric power than many other alternatives today. With the implementation of Western Development Strategy and West-East Power Transmission program, many high arch dams are under construction or will be constructed in the southwestern part of China, e.g., Jinping (305 m), XiaoWan (292 m), XiLuoDu (278 m) and Dagangshan (210 m). Due to the significant important functions in safety and economic position of high dams, these high dams may become a main object to be attacked under the war condition or to be a destructive target by terrorists. In the history of China and other countries, dam-bombing events during the war ever occurred, leading to great casualties and property loss; in the real life, the threat of dam-bombing can still be heard. Consequently, it is important to evaluate the safety of the high-arch dam against blast loading and take effective strengthening measures when necessary.

An explosion is defined as a large-scale, rapid and sudden release of energy(Hussein 2010, Shihada and Jerjawy 2011, Vijayaraghavan *et al.* 2012). Explosions can be categorized on the basis of their nature as physical, nuclear or chemical events (Ngo *et al*. 2007). The stability safe evaluation of rock like structure against explosion has been already subjected into a more attention, and some essential research results have been obtained (Børvik *et al.* 2009, Fahrenthold 1991, Feldgun *et al*. 2011, Giacomini *et al.* 2012, Khandelwal 2010, Liu *et al*. 2004, Ma *et al*. 2009, Parisi and Augenti 2012, Pandey 2010, Sanada *et al.* 2012, Sevim *et al*. 2012, Zhang 2008,

*Corresponding author, Ph.D., E-mail: scuxxh@163.com

http://www.techno-press.org/?journal=cac&subpage=8 ISSN: 1598-8198(Print), 1598-818X (Online)

Valliappan *et al.* 1990, Vestroni and Capecchi 1996, Wang *et al.* 2006, Xia *et al.* 1987, Zhu *et al.* 1997, Zhang *et al*. 2000). However, there is insufficient in evaluating the nonlinear dynamic response of a high-arch dam and therefore its failure mechanism under blast loading is still far from the state of complete clarity.

It is well known that concrete contains numerous micro-cracks or voids even before the application of any external loads. Damage in concrete is primarily caused by the propagation and coalescence of these micro-cracks or voids. Although the simplicity and efficiency of a scalar damage representation is indeed very attractive, the orientation-independent isotropic damage variable is subsequently found to be inaccurate. It has been shown that the nucleation and growth of voids as well as the orientation of fissures and their lengths observed in the process of material damage depend significantly on the direction of the applied stresses or strains and, hence, damage is in general anisotropic. Chow and Wang (Chow and Wang 1988) reported that isotropic damage models usually predict lower strength of materials compared to the theory of anisotropic damage, and the importance of the directional nature of material damage in controlling final rupture becomes more pronounced under dynamic loading conditions. An analysis without taking into account the damage-induced material anisotropy may therefore lead to questionable results.

In this paper, a damage model is developed for three dimensional analyses of arch dams. The modified Drucker-Prager criterion is adopted as the failure criteria of the damage evolution in concrete. Then, Xiluodu arch dam serves as an example to simulate the failure behaviors of structures with the proposed model. The computational results can provide a reasonable theoretical support on the safety evaluation of the capability of concrete arch dams against blast loading.

2. Anisotropic dynamic damage FEM equations

The equation of an anisotropic damaged ground under dynamic loading can be written as (Valliappan *et al.* 1990)

$$[M]\{\ddot{U}\}+[C*(\Omega(t))]\{\dot{U}\}+[K*(\Omega(t))]\{U\}=(P(t)) \tag{1}$$

Where $[M]=\int_{V_e}\rho[N]^T[N]dv$ is the mass matrix for a damaged element; [N] is the shape function matrix; $\{U\}$, $\{\dot{U}\}$, $\{\ddot{U}\}$are the displacement, velocity and acceleration vector of nodal points, respectively. $[K*(\Omega(t))]=\int_{V_e}[B]^T[T_\sigma]^T[D*][T_\sigma][B]dv$ is the time dependent stiffness matrix for an anisotropically amaged element; [D*] is the anisotropic damaged material matrix; $\{P(t)\}=\int_{s_2}[N]^T\{Q(t)\}ds+\int_{V_e}[N]^T\{F(t)\}dv$ is known as the general nodal force vector due to the pressure of foundation block, *{Q(t)* is traction vector and *{F(t)}* is body force vector; $C^*(\Omega(t))$ is the time-dependent damping matrix for a damaged element in the ground; $[T_\sigma]$is the coordinate transformation matrix defined in 3-D as

$$[T_\sigma] = \begin{bmatrix} l_1^2 & m_1^2 & n_1^2 & m_1n_1 & n_1l_1 & l_1m_1 \\ l_2^2 & m_2^2 & n_2^2 & m_2n_2 & n_2l_2 & l_2m_2 \\ l_3^2 & m_3^2 & n_3^2 & m_3n_3 & n_3l_3 & l_3m_3 \\ 2l_2l_3 & 2m_2m_3 & 2n_2n_3 & m_2n_3+m_3n_2 & n_2l_3+n_3l_2 & l_2m_3+l_3m_2 \\ 2l_3l_1 & 2m_3m_1 & 2n_3n_1 & m_3n_1+m_1n_3 & n_3l_1+n_1l_3 & l_3m_1+l_1m_3 \\ 2l_1l_2 & 2m_1m_2 & 2n_1n_2 & m_1n_2+m_2n_1 & n_1l_2+n_2l_1 & l_1m_2+l_2m_1 \end{bmatrix} \tag{2}$$

Where $\{l_i, m_i, n_i\}^{\mathrm{T}}$ are direction cosines of the normal unit vectors.

3. Dynamic damage evolution equations

For the complex analysis of dynamic damage, it is necessary to express the damage kinetic equation (growth) in the most general form as

$$\dot{\Omega} = f\left(\{\sigma_{ij}\}, \Omega, \cdots\right) \tag{3}$$

It means that the damage growth rate is related to the state of stress and damage as well as the other quantities affecting on the micro-structures in materials, in other words, the damage, stress and other quantities distributed in an element should be a function of time and position. The time and space integration of the damage kinetic equations in practical analysis is hence more difficult.

The most damage development rate models and kinetic evolutional rate equations theoretically can be applied into dynamic damage problems, but the most material parameters defined in those models and equations should be associated with the dynamical properties of dynamic loading or dynamic tests. Therefore, most investigations considered the dynamic damage equation is obtained straightly from experimental tests and expressed in the form of a power law with different stress conditions. This kind of model is more conveniently obtained by the general equipments in simple laboratory tests and more easily to be applied in various types of practical engineering with acceptable accuracy. So these kinds of damage growth models have been widely applied to the dynamic damage problems, such as the earliest model is in the form of a power law with uniform stress condition (Kachanov 1986, Zhang 1992, Zhang and Valliappan 1998)

$$\frac{d\Omega}{dt} = \begin{cases} A\left(\dfrac{\sigma}{1-\Omega}\right)^n & \sigma \geq \sigma_d \\ 0 & \sigma < \sigma_d \end{cases} \tag{4}$$

Where $A > 0$ and $n > 1$ are material constants; σ is the uniaxial stress; σ_d is the stress at damage threshold.

The most advanced improve of the model is convenient to use the concept of equivalent stress σ_{eq} of the Cauchy stress tensor $\{\sigma_{ij}\}$ in the power law for multi-axial stress state as

$$\frac{d\Omega}{dt} = \begin{cases} A\left(\dfrac{\sigma_{eq}}{1-\Omega}\right)^n & \sigma_{eq} > \sigma_d \\ 0 & \sigma_{eq} \leq \sigma_d \end{cases} \tag{5}$$

Where $A > 0$, $n > 0$ are material constants whose values depend on the rate of loading. The values of A and n can be evaluated by a general experiment, based on the three point test (Cordebois and Sidoroff 1982). The corresponding kinetic equations in the anisotropic principal axes system have the form

$$\frac{d\Omega_i}{dt} = \begin{cases} A\left(\dfrac{\sigma_{eq}}{1-\Omega}\right)^n & \sigma_{eq} > \sigma_{di} \\ 0 & \sigma_{eq} \le \sigma_{di} \end{cases} \tag{6}$$

Where the material constants $A_i > 0$, $n_i > 1$ ($i = 1, 2, 3$) can be determined by the similar experiments based on the three point test with specimens made along in the three anisotropic principal axes. σ_{eq} can be considered as an equivalent stress based on different failure criteria, such as chosen from Mohr-Coulomb or Drucker-Prager criteria and so on. σ_{di} is the threshold value of the tensile stress for the anisotropic damage growth along in the i^{th} principal direction.

In the finite element analysis, the distribution of stress and damage in an element is a nonlinear function of time and co-ordinate for complex conditions. So it is difficult to carry out the necessary integrations of kinetic equations. In order to overcome this difficulty it is proposed to introduce an average damage value $\bar{\Omega}$ and an average damage rate $\dot{\Omega}$ for isotropic case and $\bar{\Omega}_i$ and $\dot{\Omega}_i$ for anisotropic case in a specified element. Then the damage growth law in an element can be approximately developed for the isotropic case using the average value

$$\frac{d\Omega_i}{dt} = \begin{cases} \dfrac{1}{V_e}\displaystyle\int_{V_e} A\left(\dfrac{\sigma_{eq}}{1-\bar{\Omega}}\right)^n dv & \sigma_{eq} > \sigma_d \\ 0 & \sigma_{eq} \le \sigma_d \end{cases} \tag{7}$$

in which V_e is the volume of the element

Generally, the material parameters A and n are considered to be constant within an element. Thus Eq. (7) can be rewritten as

$$\frac{d\bar{\Omega}}{dt} = \begin{cases} A\dfrac{\bar{\sigma}_{eq}}{\left(1-\bar{\Omega}\right)^n} & \bar{\sigma}_{eq} > \sigma_d \\ 0 & \bar{\sigma}_{eq} \le \sigma_d \end{cases} \tag{8}$$

Where

$$\bar{\sigma}_{eq} = \frac{1}{V_e}\int_{V_e}\left(\sigma_{eq}\right)^n \mathrm{d}V \tag{9}$$

Similarly, in the case of anisotropic damage, Eq. (7) changes to

$$\frac{d\overline{\Omega}_t}{dt} = \begin{cases} \frac{1}{V_e}\int_{V_e} A \frac{A_i}{\left(1-\overline{\Omega}_i\right)^{ni}} \overline{\sigma}_i^{eq} dV & \overline{\sigma}_i^{eq} > \sigma_d \\ 0 & \overline{\sigma}_i^{eq} \le \sigma_d \end{cases} \quad (\mathrm{i}=1,2,3) \tag{10}$$

Where

$$\overline{\sigma}_i^{eq} = \frac{1}{V_e}\int_{V_e} \left(\sigma_i\right)^{n_i} \mathrm{d}V \tag{11}$$

4. Modification of drucker-prager criterion

According to the classical plasticity theory, the yield criterion determines the stress level at which plastic deformation begins. The damage plastic yield criterion can also be defined in a similar manner such that the yield condition determines the effective (net) stress level at which plastic deformation begins. This means that it is only necessary to replace the Cauchy stresses in the standard yield function by the effective stresses. The damage plastic yield function can be rewritten in the general form as

$$F(\{\sigma\},\Omega,R) = F\{\{\sigma^*\},R\} = 0 \tag{12a}$$

or

$$F(\{\sigma\},\Omega) = f\{\{\sigma^*\}\} = R(\gamma) \tag{12b}$$

where f is a function to be used to determine the effective stress level at which the plastic deformation begins. $R(\gamma)$ is the hardening function associated with the cumulative hardening parameter γ. Commonly, the hardening rule can be considered as the power rule

$$R(\gamma) = R_0 + k\gamma^{\frac{1}{m}} \tag{13}$$

The damage yield function can conveniently be expressed in the form of stress invariants as

$$f\left(I_1^*, J_2^*, J_3^*\right) = R(\gamma) \tag{14}$$

where

$$I^*{}_1 = \sigma_x^* + \sigma_y^* + \sigma_z^* = \frac{3\sigma_m}{1-\Omega} \tag{15}$$

$$J^*{}_2 = \frac{1}{2}(s_x^* + s_y^* + s_z^*) + \sigma_{yz}^*\sigma_{zy}^* + \sigma_{zx}^*\sigma_{xz}^* + \sigma_{zy}^*\sigma_{yx}^* = \frac{J_2}{(1-\Omega)^2} \tag{16}$$

$$J_3^* = Det\begin{bmatrix} s_x^* & \sigma_{xy}^* & \sigma_{xz}^* \\ \sigma_{yx}^* & s_y^* & \sigma_{yz}^* \\ \sigma_{zx}^* & \sigma_{zy}^* & s_z^* \end{bmatrix} = \frac{J_3}{(1-\Omega)^3} \tag{17}$$

For numerical computations, it is convenient to rewrite the yield function in terms of alternative stress invariants. The present formulation is modified based on Nayak and Zienkiewicz (1972) since its main advantage is that it permits the computer coding of the yield function and the flow rule in a general form and necessitates only the specification of three constants for any individual criterion. The effective principal stress vector can be given by summation of the effective deviatoric principal stress vector and the effective mean hydrostatic stress vector as

$$\begin{Bmatrix} \sigma_1^* \\ \sigma_2^* \\ \sigma_3^* \end{Bmatrix} = \frac{2\left(J_2^*\right)^{\frac{1}{2}}}{\sqrt{3}} \begin{Bmatrix} \sin\left(\theta^* - \frac{2\pi}{3}\right) \\ \sin\theta^* \\ \sin\left(\theta^* + \frac{4\pi}{3}\right) \end{Bmatrix} + \frac{I_1^*}{3} \begin{Bmatrix} 1 \\ 1 \\ 1 \end{Bmatrix} \tag{18}$$

where $\sigma_1^* > \sigma_2^* > \sigma_3^*$ and $-\pi/6 \le \theta^* \le \pi/6$. The term θ^* is essentially similar to the Lode angle.

The influence of a hydrostatic stress component on yielding was introduced by inclusion of an additional term in von Mises expression to give

$$F = \beta_o I_1^* + \left(J_2^*\right)^{\frac{1}{2}} - R(\gamma) = 0 \tag{19}$$

This yield surface has the form of a circular cone. In order to make the Drucker-Prager criterion with the inner or outer apices of the Mohr-Coulomb hexagon at any section, it can be shown that

$$\beta_o = \frac{2\sin\varphi}{\sqrt{3}(3 \pm \sin\varphi)} \tag{20}$$

$$R(\gamma) = \frac{6c\cos\varphi}{\sqrt{3}(3 \pm \cos\varphi)} \tag{21}$$

where " + " for inner apice, " – " for outer apice. Substituting Eqs. (20), (21) into Eq. (19), it gives

$$F = \frac{2\sin\varphi}{\sqrt{3}(3 \pm \sin\varphi)} I_1^* + \left(J_2^*\right)^{\frac{1}{2}} - \frac{6c\cos\varphi}{\sqrt{3}(3 \pm \cos\varphi)} = 0 \tag{22}$$

Substituting Eqs. (15) and (16) into Eq. (22), the modified Drucker-Prager criterion in terms of invariants of Cauchy stress deviator is represented as

$$F = \frac{2\sin\varphi}{\sqrt{3}(3 \pm \sin\varphi)} I_1 + \left(J_2\right)^{\frac{1}{2}} - \frac{6c\cos\varphi}{\sqrt{3}(3 \pm \cos\varphi)}(1 - \Omega) = 0 \tag{23}$$

where the cohesion c also can be equivalently expressed by the hardening rule $R(\gamma)$ as

$$c = \frac{\sqrt{3}(3 \pm \sin\varphi)}{6\cos\varphi} R(\gamma) \tag{24}$$

and when $\gamma = 0$, it gives $R|_{\gamma 0=0} = R_0$, and $c|_{\gamma 0=0} = c_0 = \sqrt{3}(3 \pm \sin\varphi)/(6\cos\varphi) R_0$, we can obtain

$$c = c_0 + \frac{\sqrt{3}\left(3 \pm \sin\varphi\right)}{6\cos\varphi} k\gamma^{\frac{1}{m}} \tag{25}$$

5. Damage analysis of the Xiluodu arch dam

5.1 Finite element mesh and material parameters

The Xiluodu hydropower station is located in the Jinshajiang River (one branch of Yangtze River). It is a huge hydropower project with comprehensive benefits of primary power generation, sediment control, flood control, downstream navigation improving. The total reservoir capacity is 12.67 billion m^3. The key structures consist of dam, power plants, flood discharge and energy dissipation structures, etc. The dam is concrete double-curvature arch type with a crest elevation of 610 m and crest length of 700 m. The maximum dam height is 278 m. Fig. 1 shows the finite element mesh of the Xiluodu arch dam, where the dam and foundation are modeled using 60725 eight-node three-dimensional solid elements. The values of material parameters adopted in the analysis are listed in Table 1, which are obtained from material tests carried out by the Chengdu Hydroelectric Investigation & Design Institute. Dynamic values of modulus of elasticity and strength are increased by 30% (Sevim *et al.* 2012). For a dynamic analysis, the damping in the numerical simulation should attempt to reproduce the energy losses in the system when subjected to dynamic loading. In rock and concrete, material damping is mainly hysteretic (i.e., independent of frequency), but it is difficult to reproduce this type of damping numerically because of the problem with path dependence. Traditionally, the typical values of intrinsic damping used by the structural engineers are 2% for steel and 5% for concrete building (Nor and Abdul 2010). Therefore, a 5% structural damping ratio is assumed in the analyses.

The exploded impact loading is assumed to be normal shock pressure on the rear surface in the downstream side of the arch dam caused by a missile (or bomb) hit. It is well known that the shot is a very complicated phenomenon, which is accompanied by a series of physical and chemical transformations. When the shot occurs, the chemical energy of gunpowder quickly turns at first into a thermal energy and then into a kinetic energy of a shell and some of mechanical parts of the gun. Part of the energy is used for operation of automatic mechanisms, and also is spent for heating of the weapon. The processes occurring in a bore at a shot are divided into four periods (Bao and Qiu 1995). The forcing period lasts from the moment of the primer-break prior to the

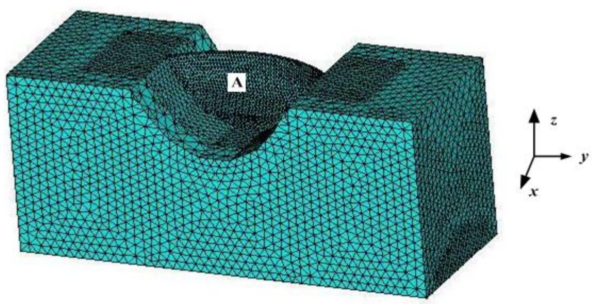

Fig. 1 Finite element model of Xiluodu arch dam

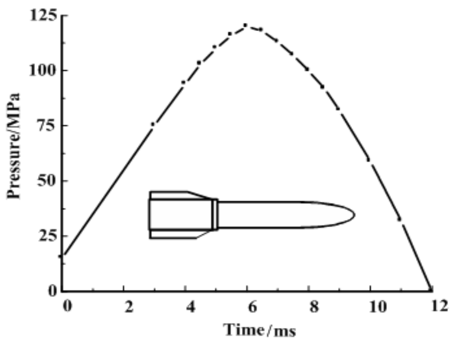

Fig. 2 Typical pressure-time history

Table 1 Material properties of xiluodu arch dam

Dam structure	E_0 (GPa)	v	ρ (kg/m^3)	f_c (MPa)	f_t (MPa)
Dam body	24.0	0.17	2400	30	2.5
Foundation rock	16.0	0.25	2600		

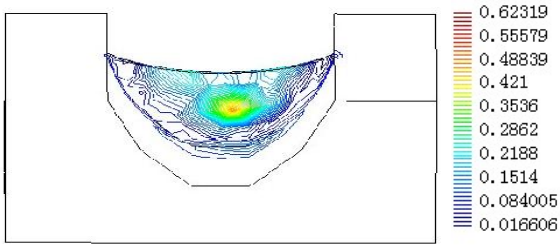

(a) Contours of Ω_x on upstream face of dam at end time

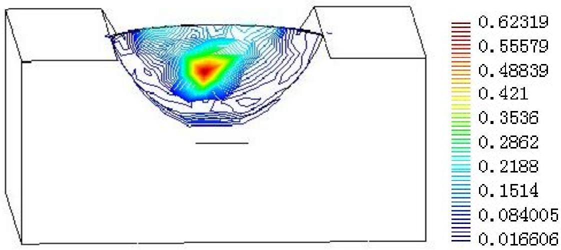

(b) Contours of Ω_x on downstream face of dam at end time

Fig. 3 Contours of Ω_x distributed on the face of upstream and downstream at end time

beginning of the motion of a shell. There is an inflaming practically by all surfaces of gunpowder grains at moment of primer-break, and then, the process of the burning is spread in the depth of the grains. At the initial moment of time the gunpowder burns in constant volume, because shell needs some energy for riping the driving band in a rifling grooves. The first ballistic period includes time from the beginning of a motion of a shell till the moment of combustion of all gunpowder and corresponds to burning of gunpowder in variable volume. In the beginning, volume, in which gunpowder is burning, is incremented slowly because the shell at this moment has small velocity,

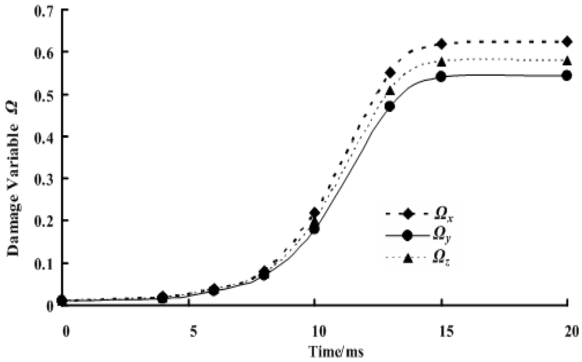

Fig. 4 Evolution history of the three principal damage variables at the point A

but the process of gas distension goes very quickly. Thus, pressure of the gunpowder-gas rapidly increases and at some moment gets of the peak value. Maximum values of gas temperature and shell acceleration also correspond to this moment. Then the shell velocity gets such value, at which the magnification of volume behind a shell goes faster, than the process of gas distension at burning gunpowder. Thus the bore pressure (pressure inside the bore) begins to decrease even before the gunpowder ends burning. The second ballistic period comes after combustion of gunpowder, when the inflow of new gases stops. However, gases which reside the space behind a shell still have a major reserve of energy. Being dilated, they keep incrementing a missile velocity. In the second ballistic period the pressure in a bore is monotonously decreases. This period comes to end when the shell leaves the barrel. The aftereffect period begins from the moment when the shell leaves the barrel and is prolonged so long as gunpowder-gases prolong to exert influence on a motion of a shell, giving it extra velocity. It can be seen that the artillery-fired missile is subjected to many kinds of loads inside the gun tube during the launch process. Of them, the powder gas pressure, called *gun pressure*, is dominant. Therefore, only the gun pressure on the bottom surface of the artillery-fired missile is taken into account in numerical analysis. A typical time history of the impulsive blast loading is given in Fig. 2.

In order to simplify the analysis, the penetration effects of the missile shot are neglected in computation. The water pressure on the surface of upstream side of the arch dam is considered in the case of a full reservoir of water. The initial anisotropic damage vectors in the dam body and batholith are assumed to be $\Omega = \{0.0, 0.0, 0.0\}^T$. The time integration scheme of dynamic equations is adopted by the Newmark's family. The values of loading parameters adopted in the analysis are as follows: the start time of computing is $t_0 = 0$ ms, the end time of computing is at $t = 40$ ms, the duration period of the shock pressure $t_s = 12$ ms, the time step is $\Delta t = 0.5$ ms, the number of total time steps is 80, and the peak pressure $P_{\max} = 120$ MPa.

5.2 Numerical results

5.2.1 Damage variables

Fig. 3 shows contours of the anisotropic principal damage variable Ω_x distributed on the face of upstream and downstream at the end of computational time, respectively. The calculated results in Fig. 3 show that the maximum damage value in stream direction may reach the quantity of $\Omega_x = 0.62319$, which appears near the loading action area. The concrete surface surrounding the point of exploded impact loading may be exfoliated due to a lot of generated micro-cracks. Since the exploded pressure area is smaller and the loading duration period is also shorter too, the localization effect of damage distribution and growth is more significant.

Fig. 4 presents the evolution history of the three principal anisotropic damage variables at the most seriously damaged position in the dam body (i.e., point A as shown in Fig. 1). It can be seen that the anisotropy of damage growth is obvious and the anisotropic principal damage variable Ω_x develops the fastest among the three principal damage variables.

5.2.2 Displacement analysis

Fig. 5 shows the contours of displacement in stream direction distributed on the face of upstream and downstream at the end of computational time, respectively. The calculated results in Fig. 5 show that the maximum displacement in stream direction may reach the quantity of u =

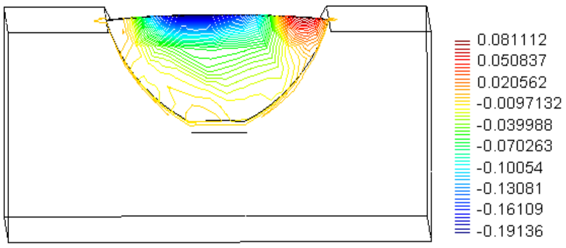

(a) Contours of *u* on upstream face of dam at end time (Unit: m)

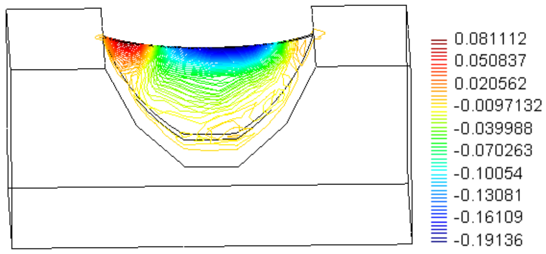

(b) Contours of *u* on downstream face of dam at end time (Unit: m)

Fig. 5 Contours of *u* distributed on the upstream face and downstream at end time

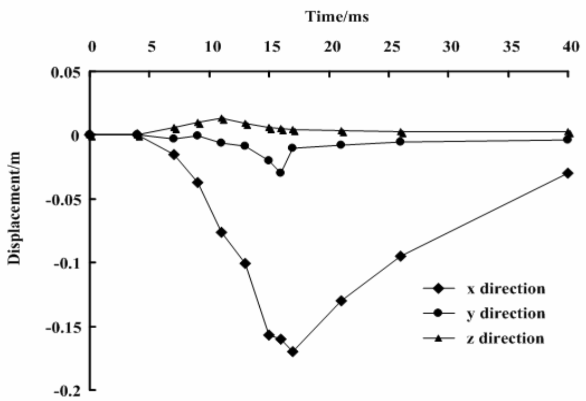

Fig. 6 Evolution history of the three displacements at the point A

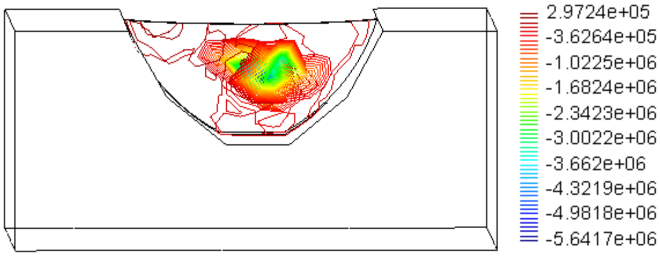

(a) Contours of σ_x on upstream face of dam at t=10ms (Unit: Pa)

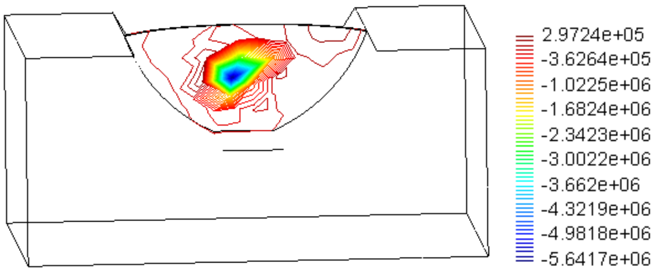

(b) Contours of σ_x on downstream face of dam at t=10ms (Unit: Pa)

Fig. 7 Contours of σ_x distributed on the face of upstream and downstream at t=10ms

19.136 cm which appears at the crest of the dam.

Fig. 6 presents the evolution history of the three displacements at the most seriously damaged position in the dam body (i.e., point A as shown in Fig. 1). It can be seen that the anisotropy of displacement is also obvious and the displacement in stream direction develops the fastest among the three displacements.

5.2.3 Stress analysis

Fig. 7 shows contours of stress σ_x distributed both on the back surface of down stream side and on the surface of upper stream side at the time t = 10 ms of loading peak, respectively. It can be seen that the phenomenon of stress concentration is quite distinctness. The stress state on the back surface of down stream side still is a pressure state priority, whereas the stress state on the surface of upper stream side may become tensile. Therefore, during loading time, the dynamic stress state diffuses towards the inside the dam body and batholiths, the stress in the centre area of stress concentration increases firstly then decreases secondly due to attenuations of the shock loading density.

5.2.4 Discussion of results

The results show that the serious damage appears at the position of the dam back near the load range where the dam surface is much easier to damage. The peak value and the duration time of the blast-impact load have an important influence to damage growth and damage propagation. Because the duration period of the blast load lasted very short, the localization of the damage is quite significant. When the dynamic stress due to the impact load is higher than that of the threshold value of damage developing in the material, the damage in the material would be sharply grow, that may extremely adverse to the safety of structure.

Besides, in this analysis, the model of an exploded blasting impact load due to a missile attack does not involve the penetration effect of the missile attack during a strike on the dam body. The damage behavior from penetration effects due to missile attack during strikes on concrete targets should be studied in the future work.

6. Conclusions

A damage model has been developed for 3-D analysis of arch dams in this paper. The modified Drucker-Prager criterion is adopted as the failure criteria of the damage evolution of concrete. Then, Xiluodu arch dam serves as an example to simulate the failure behaviors of structures with the proposed model. From these studies, following conclusions and understandings may be drawn

1) The modified Drucker-Prager criterion proposed in this paper are effective and feasible in analyzing the dynamic response of an arch dam subjected to blast loading.

2) The concrete surface surrounding the point of exploded impact loading may be exfoliated due to a lot of generated micro-cracks. Since the exploded pressure area is smaller and the loading duration period is also shorter, the localization effect of damage distribution and growth is more significant.

3) The anisotropy of damage growth is very obvious and the anisotropic principal damage variable along stream direction develops the fastest among the three principal damage variables.

4) The anisotropy of displacement is also very obvious and the displacement in stream direction develops the fastest among the three displacements.

References

Bao, T.Y. and Qiu, W.J. (1995), *Interior Ballistic*, Beijing Institute of Technology Press, Beijing.

Børvik, T., Hanssen, A.G., Langseth, M. and Olovsson, L. (2009), “Response of stuctures to planar blast loads - A finite element engineering approach”, *Comput. Struct.*, **87**(9-10), 507-520.

Cordebois, J.P. and Sidoroff, F. (1982), “Endommagement anisotropic”, *J. Theor. App. Mech.*, **1**(4), 45-60.

Chow, C.L. and Wang, J. (1988), “A finite element analysis of continuum damage mechanics for ductile fracture”, *Int. J. Fracture*, **38**, 83-102.

Feldgun, V.R., Karinski, Y.S. and Yankelevsky, D.Z. (2011), “A simplified model with lumped parameters for explosion venting simulation”, *Int. J. Impact Eng.*, **38**(12), 964-975.

Parisi, F. and Augenti, N. (2012), “Influence of seismic design criteria on blast resistance of RC framed buildings: A case study”, *Eng. Struct.*, **44**, 78-93.

Pandey, A.K. (2010), “Damage prediction of RC containment shell under impact and blast loading”, *Struct. Eng. Mech. Int. J.*, **36**(6), 729-744.

Fahrenthold, E.P. (1991), “A continuum damage model for fracture of brittle solids under dynamic loading”, *J. Appl. Mech.-T., ASME*, **58**, 904-909.

Giacomini, A., Thoeni, K., Lambert, C., Booth, S. and Sloan, S.W. (2012), “Experimental study on rockfall drapery systems for open pit highwalls”, *Int. J. Rock Mech. Min.*, **56**,171-181.

Hussein, A.T. (2010), “Non-linear analysis of SDOF system under blast load”, *Eur. J. Sci. Res.*, **45**(3), 430-437.

Kachanov, L.M. (1986), *Introduction to continuum damage mechanics*, Martinus Nijhoff Publishers, Brookline MA02146, USA.

Khandelwal, M. (2010), “Evaluation and prediction of blast-induced ground vibration using support vector machine”, *Int. J. Rock Mech. Min.*, **47**(3), 509-516.

Liu, Y.Q., Li, H.B. and Li, J.R. (2004), “UDEC simulation on dynamic response of rock slope of

huangmailing phosphorite mine under explosion", *Chin. J. Rock Mech. Eng.*, **23**(21), 3659-3663.
Ma, G.W., Huang, X. and Li, J.C. (2009), "Damage assessment for buried structures against internal blast load", *Struct. Eng. Mech., An Int. J.*, **32**(2), 301-320.
Ngo, T., Mendis, P., Gupta, A. and Ramsay, J. (2007), "Blast loading and blast effects on structures-an overview", *EJSE Special Issue: Loading on Structures*, 76-91.
Nayak, G. and Zienkiewicz, O.C. (1972), "Convenient form of stress invariants for plasticity", *J. Struct. Div. ASCE*, 949-953.
Nor, H. and Abdul, H. (2010), "A concept development and proposed design procedure for rocking precast hollow core wall in warehouse", *J. Inst.Eng.*, **71**(2), 18-26.
Shihada, S.M. and Jerjawy, M.A. (2011), "Assessment and strengthening of a sixteen storey RC building damaged by air attack", *The Islamic University Journal (Series of Natural Studies and Engineering)*, **19**(2), 37-56.
Sanada, H., Nakamura, T. and Sugita, Y. (2012), "Mine-by experiment in a deep shaft in Neogene sedimentary rocks at Horonobe, Japan", *Int. J. Rock Mech. Min.*, **56**, 127-135.
Sevim, B., Altunisik, A.C., Bayraktar, A., Akkose, M. and Adanur, S. (2012), "Estimation of elasticity modulus of a prototype arch dam using experimental methods", *J. Mater. Civil Eng., ASCE*, **24**(4), 321-329.
Sevim, B., Altunisik, A.C. and Bayraktar, A. (2012), "Experimental evaluation of crack effects on the dynamic characteristics of a prototype arch dam using ambient vibration tests", *Comput. Concrete, An Int. J.*, **10**(3), 277-294.
Valliappan, S., Zhang, W.H. and Murti, V. (1990), "Finite element analysis of anisotropic damage mechanics problems", *Eng. Fract. Mech.*, **35**, 1061-1071.
Vijayaraghavan, C., Thirumalaivasan, D. and Venkatesan, R. (2012), "A study on nuclear blast overpressure on buildings and other infrastructures using geospatial technology", *J. Comput. Sci.*, **8**(9), 1520-1530.
Vestroni, F. and Capecchi, D. (1996), "Damage evaluation in vibrating beams using experimental frequencies and finite element models", *J. Vib. Control*, **2**, 69-86.
Wang, S.S., Ren, Q.W. and Qiao, P.Z. (2006), "Structural damage detection using local damage factor", *J. Vib. Control*, **12**, 955-973.
Xia, X., Li, H.B. and Li, J.R. (1987) "Numerical simulation of blast-induced cracks in rock", *Rock Soil Mech.*, **27**(11),1987-1991.
Zhang, L. (2008), "The research of crack extending in rock under blast loading", *J. Huinan Vocational Tech. College*, **8**(1),15-16.
Zhu, C.Y., Lu, W.B. and Dong, Z.H. (1997), "Summary of control standard for rock slope under blasting vibration", *Blasting*, **14**(4), 13-17.
Zhang, W.H., Chen, Y.M. and Jin, Y. (2000), "A Study of Dynamic Responses of Incorporating Damage Materials and Structure", *Struct. Eng. Mech., Int. J.*, **12**(2), 139-156.
Zhang, W.H. (1992), "Numerical Analysis of Continuum Damage Mechanics", Ph.D. Thesis, University of New South Wales, Australia.
Zhang, W.H. and Valliappan, S.(1998), "Continuum damage mechanics theory and application-part I: theory; part II-application", *Int. J. Damage Mech.*,**7**, 250-273.

CC